Studies in binary nucleation: The dibutylphthalate/dioctylphthalate system

Kikuo Okuyama and Yasuo Kousaka
Department of Chemical Engineering, University of Osaka Prefecture, Osaka, Japan
Sonia Kreidenweis, Richard C. Flagan, and John H. Seinfeld[a)]
Department of Chemical Engineering, California Institute of Technology, Pasadena, California 91125

(Received 3 November 1987; accepted 9 August 1988)

A continuous-flow mixing apparatus has been developed for the study of binary nucleation. This apparatus has been used to investigate the nucleation of mixed dibutylphthalate/dioctylphthalate vapors, and the interaction of the two vapors in particle formation has been demonstrated. A model that considers competition between nucleation and condensation processes during particle formation is applied in the analysis of the experimental results, allowing comparison of the magnitudes of the theoretical and actual nucleation rates in both the single-component and mixed vapor systems.

I. INTRODUCTION

The formation of particles by homogeneous nucleation from a vapor phase containing two condensable components, so-called binary nucleation, has received much attention from both theoretical and experimental points of view. The most distinctive aspect of binary nucleation is the formation of particles at supersaturations of either component that are insufficient to support significant homomolecular homogeneous nucleation.

Previous theoretical analyses of particle formation in two-component systems have been, for the most part, based on modifications of the original theory for binary nucleation as developed by Reiss.[1] This theory is an extension of the classical homomolecular (Becker–Döring–Zeldovich) nucleation theory to two components, and contains similar inherent assumptions (e.g., the equilibrium cluster distribution assumption and determination of the critical cluster size by equating liquid- and gas-phase chemical potentials, allowing for the change in free energy due to formation of the interface). Supersaturations with respect to the composition over a solution droplet are smaller (or larger) than those with respect to a pure phase, depending on the deviation from ideality of the solution behavior. The critical cluster size, and hence nucleation rate, are greatly affected by such nonidealities. The classical example of greatly enhanced nucleation due to solution nonidealities is the sulfuric acid–water system, for which large rates of nucleation have been theoretically predicted at low relative humidities and for trace amounts of acid vapor.

Limited data are available with which to evaluate the theories; most laboratory studies of binary nucleation have been carried out using equipment originally developed for the study of homomolecular nucleation, such as the piston cloud chamber,[2] the diffusion cloud chamber,[3] and the supersonic nozzle.[4] These systems allow one to determine the critical supersaturation ratio for nucleation, but usually do not give information about the dependence of the aerosol number concentration on the supersaturations of the two component vapors. An additional disadvantage is that those which rely on expansion to produce supersaturations operate at low temperatures.

Recently, the device referred to as the particle size magnifier (PSM) has been employed[5,6] to study the homogeneous nucleation of single-component vapors without introducing the complications inherent in many of the traditional systems. In the PSM, a saturated, high-temperature vapor stream is rapidly mixed with room-temperature gas to generate large supersaturations, with nucleation and growth subsequently occurring in an isothermal region downstream. A wide range of saturation ratios and mixed temperatures in a range of atmospheric interest (e.g., 30 °C), can be achieved by adjusting the temperatures and relative flow rates of the streams. By observing the total number of particles produced for various supersaturations, both the critical supersaturation and the dependence of the number of particles formed upon saturation ratio can be determined. This dependence can be related to that predicted theoretically using an appropriate model. Experiments performed in a PSM, therefore, can potentially yield more information about the nucleation process, especially at conditions of atmospheric interest, than those performed using other types of apparatus.

We present here the first measurements of binary nucleation rates in the particle size magnifier. Two organic species, dibutylphthalate (DBP) and dioctylphthalate (DOP), were chosen for this study. Previous single-component experiments in the PSM[5,6] investigated the homomolecular nucleation behavior of DBP, and a number of other researchers have studied nucleation of either of these compounds. Advantages of this choice of species include the following: Most of the physical properties of both compounds are known, and since they are similar organics they are expected to form ideal solutions, thus simplifying the theoretical analysis. Because of the low saturation vapor pressures, the droplets formed are expected to be stable, minimizing losses during the counting.

The experimental procedure used in this study was designed to allow for direct comparison between the numbers of particles produced in the case of mixed vapor and those

a) To whom correspondence should be addressed.

 0021-9606/88/226442-12$02.10 © 1988 American Institute of Physics
Downloaded 21 Dec 2005 to 131.215.225.171. Redistribution subject to AIP license or copyright, see http://jcp.aip.org/jcp/copyright.jsp

that would have been produced in the presence of either species alone. This was achieved by performing a mixed vapor experiment at a particular set of temperatures and flow rates, then replacing in turn each of the organic vapor streams by a dry air stream and repeating the experiment at the same conditions, but in the presence of only one of the condensable vapors. The number of droplets formed via the different nucleation mechanisms is measured and compared with those predicted from a dynamic model that combines expressions for classical nucleation and steady-state particle growth.

II. EXPERIMENTAL APPARATUS AND METHOD

Figure 1 shows a schematic of the experimental apparatus used in the binary nucleation experiments, which is similar to that used in the previous nucleation studies of single-component DBP vapor. A high purity, particle-free air stream is split into three gas flows: one is a room temperature diluent gas flow and the other two are high temperature carrier gas flows that are saturated with either DBP or DOP vapor after passing through each saturator. The two high temperature flows are preliminarily mixed. The resulting DBP–DOP vapor flow is turbulently mixed with the room temperature flow in the mixing unit, and then held at constant temperature through the residence volume, where the supersaturated vapor is given time to homogeneously nucleate. The resulting aerosol stream then goes to particle measurement instrumentation.

Each saturator consists of a column filled with silica gel that has been impregnated with liquid DBP or DOP as shown in Fig. 2. The flow rate of carrier air may range from 0.1 to 0.5 ℓ/min. Temperatures measured by alumel–chromel thermocouples at five positions in the saturators were consistent to within 0.1 °C.

Figure 3 depicts the mixing unit that is used to rapidly mix the high temperature DBP–DOP vapor with low-temperature diluent gas. The temperatures of the DBP and DOP streams are denoted T_{sh1} and T_{sh2}, respectively, and T_l represents the temperature of the diluent gas flow. The particle-free air saturated with the organic vapors flows horizontally into a tube and meets low-temperature gas blown in through eight 0.08 cm diameter holes. The flow rates of the vapor streams from each saturator are denoted Q_{sh1} and Q_{sh2}, and

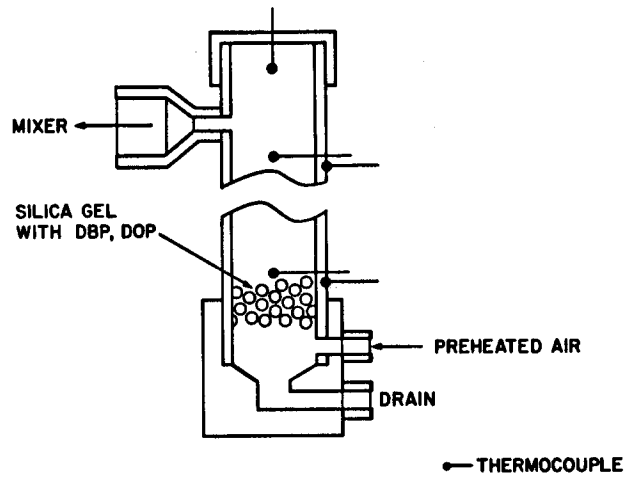

FIG. 2. Schematic of saturator.

the flow rate of room-temperature gas is Q_l. The mixing ratios, R_{h1} and R_{h2}, are expressed as Q_{sh1}/Q_m for DBP and Q_{sh2}/Q_m for DOP, where Q_m is the total flow rate of mixed gas. For these experiments, a mixing ratio of either 0.1 or 0.2 was used for both R_{h1} and R_{h2}. The vapor temperatures from the saturators were varied from 100 to 155 °C, and the flow rate of room-temperature gas Q_l ranged from 0.8 to 2.0 ℓ/min.

The residence volume unit, which shall be referred to as the reheater, consists essentially of a temperature-controlled tube. The DBP–DOP vapor and air mixture flows from the mixing unit directly into the reheater, which provides the desired residence time t_r for homogeneous nucleation and condensational growth to occur. A temperature controller is used to maintain the temperature T_r equal to the adiabatic mixing temperature of the vapor–air stream, T_m, in order to maintain constant conditions for nucleation. In the case of DBP and DOP vapors, the vapor pressures and latent heats are sufficiently small that the increase in temperature of the gas after condensation is negligible, so that the temperature of the reheater can be maintained constant down its length.

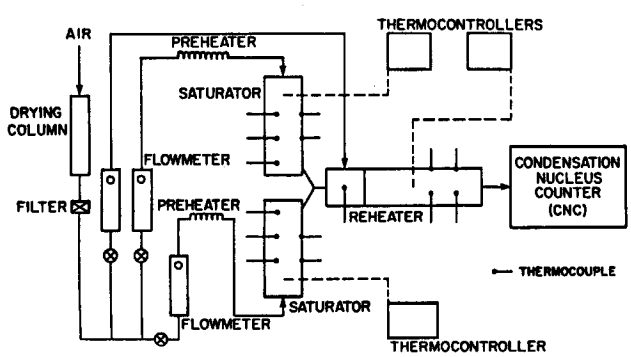

FIG. 1. Schematic of experimental apparatus.

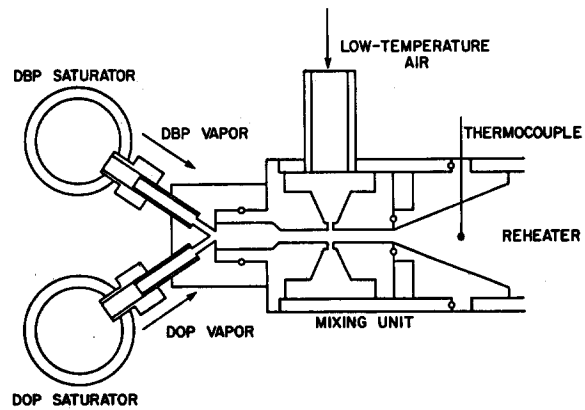

FIG. 3. Schematic of mixing unit.

Downloaded 21 Dec 2005 to 131.215.225.171. Redistribution subject to AIP license or copyright, see http://jcp.aip.org/jcp/copyright.jsp

TABLE I. Property data for DBP and DOP.

	DBP	DOP
Molecular weight	278.35	390.56
Vapor pressure[a] (Torr)	$\ln p = 16.27 - \frac{5099}{T + 163.5}$	$\ln p = 29.31 - \frac{13408}{T + 273.15}$
Density[a] (g cm^{-3})	$1.063 - 0.00083\,T$	0.98
Surface tension[a] (dyn cm^{-1})	$35.3 - 0.0863\,T$	$32.2 - 0.0737\,(T - 25)$

[a] T in °C.

The volume of the reheater is 190 cm^3, giving a residence time of 5.7 s for a gas flow rate $Q_m = 2$ *l*/min. Part of the total flow is drawn through a TSI 3020 condensation nucleus counter (CNC), which measures the total particle number concentration.

In starting up the PSM, the three air flows were first set to the desired values, and the temperatures of the saturators were increased gradually to the desired values. The temperature of the reheater was simultaneously controlled so that it would be at the mixed temperature determined by heat and mass balances. Assuming that the hot air–vapor mixture is combined rapidly and adiabatically with the room temperature air, in the supersaturated atmosphere produced, the temperature of the mixed gas T_m and the absolute masses of DBP and DOP per kilogram of dry air, H_{m1} and H_{m2}, respectively, are given by heat and mass balance equations:

$$T_m = (C_{sh1} T_{sh1} Q_{sh1} + C_{sh2} T_{sh2} Q_{sh2} + C_l Q_l T_l)/C_{si} Q_T, \quad (1)$$

$$H_{m1} = H_{sh1} Q_{sh1}/Q_T, \quad (2)$$

$$H_{m2} = H_{sh2} Q_{sh2}/Q_T, \quad (3)$$

$$Q_T = Q_{sh1} + Q_{sh2} + Q_l, \quad (4)$$

where C is the specific heat, kcal/kg (dry air) K, Q the mass flow rate, kg(dry air)/s, and the vapor content H can be related to the vapor pressure of DBP or DOP, p in mm Hg:

$$H = Mp/[28.966(760 - p)]. \quad (5)$$

The saturation ratios S_{01} and S_{02} for DBP and DOP vapors can be found from

$$S_{01} = p_1/p_1^0, \quad S_{02} = p_2/p_2^0, \quad (6)$$

where p_1^0 and p_2^0 are the saturated vapor pressures of DBP and DOP at the temperature T_m. In the calculation of these saturation ratios, the physical properties listed in Table I were used.

Figure 4 shows the values of the initial saturation ratios S_0 in the mixing zone for both DBP and DOP vapors. It can be seen that the value of S_0 depends strongly on the temperatures of both gas streams and on the mixing ratio. It is also seen that S_0 attains high values when R_h is between 0.05 and 0.3. For the same temperatures and mixing conditions, DOP attains higher values of S_0 than does DBP, due to the higher boiling point of DOP. A relatively small value of R_h (0.1) was selected to maintain the temperature of the mixed gas only slightly above room temperature. This ratio led to high supersaturations in the reheater and prevented a significant temperature drop between the reheater and the room temperature detector, which could have led to additional homogeneous nucleation.

In the experiment, a particular set of flow rates was used for all the runs; the variation in saturation ratio was achieved by changing the temperatures of the vapor streams, T_{sh1} and T_{sh2}. These were selected so that there was no possibility of particle formation during the preliminary mixing process, before dilution with cool air. The number concentration of homogeneously nucleated binary droplets was measured at steady state. By then replacing one saturator containing the impregnated silica gel with one filled with dry gel, homogeneous nucleation of a single-component vapor was observed for comparison with binary nucleation at the identical temperatures and mixing conditions.

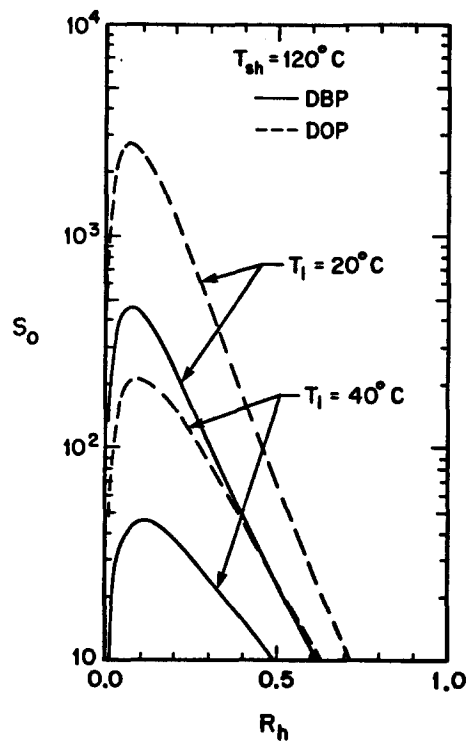

FIG. 4. Initial saturation ratio S_0 as a function of mixing ratio for two dilution temperatures.

Downloaded 21 Dec 2005 to 131.215.225.171. Redistribution subject to AIP license or copyright, see http://jcp.aip.org/jcp/copyright.jsp

A typical set of experimental data is given in Table II. In all the experiments, the flow through each saturator was one-tenth of the total mixed flow rate (as indicated by $R_{h1} = R_{h2} = 0.1$), and the dilution air stream temperature was approximately 21 °C. This condition resulted in a mixed-gas temperature T_m of approximately 42 °C. For the particular experiment of Table II, the temperature of the DOP saturator remained fixed at 130 °C as the temperature of the DBP saturator was increased stepwise. The first block of data shows results in the mixed-vapor cases; in the second block, the DOP saturator was replaced by a dry column, resulting in nucleation of DBP particles; and in the third, the DBP column was replaced by dry gel. These data are shown as a function of the saturation ratio of DBP in Fig. 5, with the closed circles representing the binary results, and the closed squares and triangles representing homomolecular DBP and DOP nucleation, respectively. It is not possible to also show the saturation ratio of DOP; the homomolecular DOP results are shown as a function of the saturation ratio of DBP that would have been obtained if the DBP saturator had not been replaced by a dry column.

It is immediately evident from Fig. 5 that the numbers of particles produced in the mixed-vapor case cannot be explained by homogeneous nucleation of DBP or DOP alone. However, as the saturation ratio of DBP becomes very small or very large, the mixed-vapor results tend towards those for single-component nucleation. Both of these observations support qualitatively the predictions of binary nucleation theory. In the next section we present a model to be used for quantitative comparisons.

TABLE II. Experimental conditions and measured number concentrations.

$R_{h1} = R_{h2} = 0.1$				$T_{sh2} = 130$ °C	
T_{sh1}	T_l	T_m	S_{01}	S_{02}	N
100	21.0	39.8	30.8	1454.0	2.784×10^5
104	21.0	40.2	39.1	1376.3	2.292×10^5
108	21.8	41.3	45.6	1194.2	2.088×10^5
112	22.0	41.8	56.0	1106.4	1.186×10^5
116	20.8	41.3	78.0	1192.7	1.236×10^5
120	21.0	41.8	94.2	1104.6	3.018×10^5
124	20.4	41.8	122.2	1115.3	5.496×10^5
128	21.0	42.7	139.8	988.9	7.886×10^5
132	21.2	43.2	165.4	915.5	2.248×10^6
124	21.2	42.4	113.0	···	1.140×10^2
126	21.2	42.6	124.6	···	5.582×10^2
128	21.0	42.5	142.5	···	3.258×10^3
130	21.0	42.9	153.7	···	3.082×10^4
132	21.0	43.1	168.6	···	9.220×10^4
134	21.2	43.4	181.2	···	6.932×10^5
136	21.0	43.5	202.0	···	8.750×10^6
100	20.0	39.0	···	1622.8	1.140×10^2
108	20.0	39.8	···	1453.0	5.582×10^2
116	20.4	40.9	···	1245.7	3.258×10^3
120	20.8	41.7	···	1128.8	3.082×10^4
124	21.0	42.2	···	1045.3	9.220×10^4
128	21.4	43.0	···	947.4	6.932×10^5
132	21.6	43.5	···	877.1	8.750×10^6
136	21.8	44.1	···	811.9	8.750×10^6

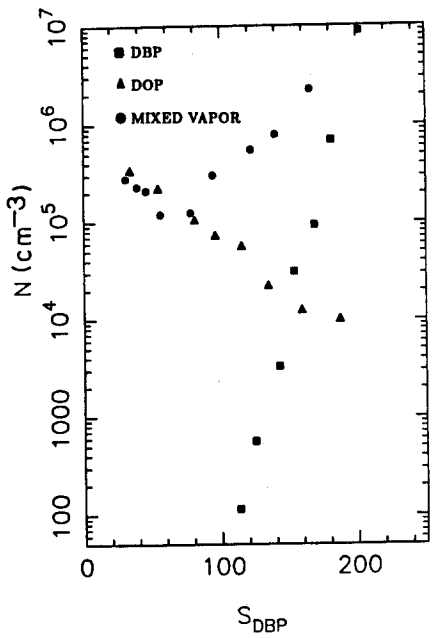

FIG. 5. Total number concentrations of particles for DBP-only, DOP-only, and mixed-vapor cases, $T_{sh2} = 130$ °C.

III. INTEGRAL MODEL FOR BINARY NUCLEATION AND GROWTH

To analyze the measured particle number concentrations for both single-component and binary nucleation, one must account for nucleation, depletion of the vapor, and growth of particles by condensation. An integral model, for example that developed by Warren *et al.*[7,8] for single-component particles, and extended to binary systems by Kreidenweis and Seinfeld,[9] can be used. In such an integral model it is assumed that the total number of aerosol particles is divided into sets; each set consists of monodisperse particles at a specified diameter, and is referred to as a mode and is given the index i. For example, if there are preexisting particles in the system of diameter d_{p_1} and new particles of diameter d_{p_2} are nucleated, two modes are used in describing the aerosol. (No preexisting particles were present in the experiments reported here.) The aerosol is further described by its moments, total number concentration in each mode N_i and total mass concentration of each condensable species in each mode M_{ji} and the vapor phase by the saturation ratio of each species S_j.

The condensation rate of each component j is approximated by a continuum expression modified for noncontinuum effects by the expression developed by Dahneke,[10] and incorporating a factor α that accounts for polydispersity and is defined by

$$R_{c_{ij}} = \frac{2\pi D_j p_j^0}{RT} \int_{d_{p_i}^*}^{\infty} d_{p_i} \left[S_j - a_{ji} \exp\left(\frac{4\sigma \bar{V}_j}{d_{p_i} RT} \right) \right] \times n_i(d_{p_i}) f(Kn_{ji}) dd_{p_i} \tag{7}$$

Downloaded 21 Dec 2005 to 131.215.225.171. Redistribution subject to AIP license or copyright, see http://jcp.aip.org/jcp/copyright.jsp

$$= \alpha_{ji} N_i \left\{ \frac{2\pi D_j p_j^0}{RT} \overline{d_{p_i}} \left[S_j - a_{ji} \exp\left(\frac{4\sigma \overline{V}_j}{\overline{d_{p_i}} RT} \right) \right] \times f(\overline{Kn_{ji}}) \right\}, \quad (8)$$

$$f(Kn_{ji}) = \frac{1 + Kn_{ji}}{1 + 2Kn_{ji}(1 + Kn_{ji})}, \quad (9)$$

$$Kn_{ji} = \frac{2\lambda_j}{d_{p_i}},$$

where D_j is the diffusion coefficient of species j in the mixture, d_{p_i} is the particle diameter, a_j is the activity of species j in the solution, σ is the surface tension, $\overline{V}_j$ is the partial molar volume of species j, Kn_{ji} is the Knudsen number, and λ_j is the mean free path of species j. The polydispersity factor α_{ji} is somewhat less than one, but will be taken as equal to one in these simulations. This assumes the aerosol to be monodisperse and will tend to somewhat overpredict the condensation rate, thus underpredicting the total number of particles formed. The significance of α is discussed in more detail in the Appendix.

The rate of formation of particles will be described by the binary nucleation rate expression of Mirabel and Katz,[11] as modified by Stauffer,[12]

$$R_{J_{\mathrm{BIN}}} = C_J \exp(-\Delta G^*/kT), \quad (10)$$

$$\Delta G^* = \tfrac{4}{3}\pi\sigma r^{*2}, \quad (11)$$

$$C_J = \frac{\beta_1\beta_2}{\beta_1 \sin^2\phi + \beta_2 \cos^2\phi} \frac{(S_1 p_1^0 + S_2 p_2^0)}{kT} 4\pi r^{*2} Z, \quad (12)$$

where β_i is the impingement rate of species i onto the cluster of radius r^*, ϕ is the angle between the unrotated coordinates and the rotated coordinates through the saddle point, and Z is the binary Zeldovitch factor. These expressions are directly analogous to those for the single-component case. The quantities Z and ϕ are determined from the second derivatives of the free energy:

$$\tan\phi = s + (s^2 + \beta_1/\beta_2])^{1/2}, \quad (13)$$

$$s = \frac{1}{2}\left[\left(\frac{\partial^2 \Delta G}{\partial n_1^2} - \frac{\beta_1}{\beta_2} \frac{\partial^2 \Delta G}{\partial n_2^2} \right) \Big/ \frac{\partial^2 \Delta G}{\partial n_1 \partial n_2} \right], \quad (14)$$

$$Z = \left[-\left(\frac{\partial^2 \Delta G}{\partial n_1^2} \cos^2\phi + \frac{\partial^2 \Delta G}{\partial n_2^2} \sin^2\phi + 2 \frac{\partial^2 \Delta G}{\partial n_1 \partial n_2} \cos\phi \sin\phi \right) \right] \Big/ \left[\left(\frac{\partial^2 \Delta G}{\partial n_1 \partial n_2} \right)^2 - \frac{\partial^2 \Delta G}{\partial n_1^2} \frac{\partial^2 \Delta G}{\partial n_2^2} \right]^{1/2}. \quad (15)$$

It was assumed for this study that DBP and DOP form ideal solutions,[13] which is expected to be a reasonable estimate for two similar organic compounds. Therefore, the partial molar volumes are equal to the molar volumes of the pure components. It was also assumed that the vapor pressure of the solution obeys Raoult's law over the complete composition range, so that the activity of each component in solution is equal to its mole fraction. Due to lack of solution data, a simple linear relation was assumed for the mixture surface tension:

$$\sigma = x_{\mathrm{DBP}}\sigma_{\mathrm{DBP}} + x_{\mathrm{DOP}}\sigma_{\mathrm{DOP}}.$$

The assumption that DBP and DOP form ideal solutions can be invoked to simplify the equations used to determine the properties of the critical cluster. For ideal binary solutions ($j = 1,2$), the composition of the critical embryo can be determined by

$$\ln\frac{S_2}{x_2} = \ln\left\{ \frac{S_1}{x_1} \left[\left(V_2 + \frac{3}{2}\frac{V}{\sigma} x_1 \frac{d\sigma}{dx_2} \right) \Big/ \left(V_1 - \frac{3}{2}\frac{V}{\sigma} x_2 \frac{d\sigma}{dx_2} \right) \right] \right\}, \quad (16)$$

which defines the critical size to be

$$r^* = \left(2\sigma V_1 - 3x_2 V \frac{d\sigma}{dx_2} \right) \Big/ [RT \ln(S_1/x_1)]. \quad (17)$$

Recent work[14] has suggested that the surface tension derivatives should not be included in Eqs. (16) and (17). The effect of this revision was checked by repeating some of the simulations presented in this work with the surface tension derivatives set equal to zero. The resulting number concentrations were lower than those obtained using Eqs. (16) and (17) by less than a factor of 3.

One difficulty with the binary nucleation rate expression, which was pointed out by Wilemski,[15] is the failure to approach the classical single-component rate as the supersaturation of either component approaches zero. This behavior is attributed to the divergence of the nonequilibrium (Zeldovitch) term as the curvature of the free energy surface, in the denominator, becomes undefined. Our approach to this problem follows the suggestion of Mirabel and Clavelin.[16] First, Eqs. (16) and (17) were used to determine the number of molecules of each species in the critical cluster. If one of these was found to be less than one, it was assumed that single-component nucleation, not binary, would occur. The homomolecular nucleation rate was taken to be the classical Becker–Döring–Zeldovitch rate:

$$R_j = S_j^2 \left(\frac{p_j^0}{kT} \right)^2 2v_j \left(\frac{\sigma_j}{2\pi m_j} \right)^{1/2} \exp\left(\frac{-16\pi\sigma_j^3 v_j^2}{3k^3 T^3 \ln^2 S_j} \right). \quad (18)$$

Insight into the theoretical behavior of binary nucleating systems can be gained by considering a simplified ideal mixture of two species $A(j = 1)$ and $B(j = 2)$ that will be considered to have the same physical properties, including vapor pressure. Therefore, the composition and size of the critical cluster are given by

$$x_1 = \frac{S_1}{S_1 + S_2} \quad (19)$$

$$r^* = \frac{2\sigma V}{RT \ln(S_1/x_1)}. \quad (20)$$

Nonidealities of solution behavior affect the free energy of formation of the embryo. The effect of varying the formation free energy from that of an ideal system,

$$\Delta G = kT(x_1 \ln x_1 + x_2 \ln x_2) \quad (21)$$

is shown in Fig. 6 for the hypothetical A–B system. The single-component nucleation rates are also shown for comparison. It is immediately seen from Fig. 6 that the ideal binary

Downloaded 21 Dec 2005 to 131.215.225.171. Redistribution subject to AIP license or copyright, see http://jcp.aip.org/jcp/copyright.jsp

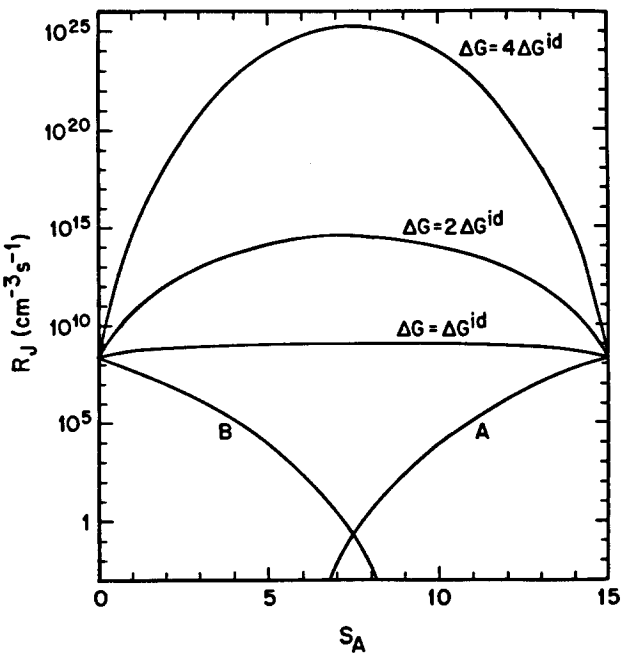

FIG. 6. Single-component and binary nucleation rates in an idealized *A–B* system with various assumptions for free energy of mixing.

system behaves as though a single component were present: the nucleation rate is constant and equal to the rate expected for a saturation ratio equal to the sum of the individual ratios, $S_1 + S_2$. Therefore, considering binary nucleation of two similar species leads to a larger predicted rate than would be expected for either species alone. Also, if the two species form a (favorably) nonideal solution, even larger rates are predicted by binary nucleation theory. The shape of the curves will be somewhat different for *A* and *B* having different physical properties (as is the case with DBP–DOP).

For modeling the DBP–DOP single-component and mixed-vapor experiments, a number of inputs are required. First, the initial saturations in the mixing chamber S_{j_0} are evaluated at the adiabatic mixing temperature calculated for the experimental conditions. This temperature is assumed constant throughout the nucleation and growth processes, neglecting the effects of latent heats, heats of mixing, and possible radial variations in the flow tube.

No seed particles were introduced into the mixed vapor stream, and therefore we need consider only one mode containing the nucleated particles. We can therefore omit the subscript *i*. In order to compute the mean diameter required for evaluation of Eq. (8), it is assumed that the mass of each component per particle can be estimated by M_j/N. These masses, with the density of the solution, are used to obtain the diameter.

The rate of generation of new particles is given by Eq. (10) in the mixed-vapor cases, and by Eq. (18) when only one vapor is present; the appropriate source term is denoted by R_J in the equations that follow. The condensation rate for each component is given by Eq. (8). The remaining variables in the integral model are the saturation ratios of each condensable species. The total particle number concentration N varies due only to nucleation; the total particle mass concentration $M_j, j = 1,2$, varies from both nucleation and condensation; and the saturation ratios $S_j, j = 1,2$, of each species decreases as gas-to-particle conversion takes place. The integral model expresses these changes by

$$\frac{dN}{dt} = R_J E_J, \tag{22}$$

$$\frac{dM_j}{dt} = MW_j\left(g_j^* \frac{dN}{dt} + R_{C_j}\right), \tag{23}$$

$$S_j(t) = S_{j_0} - M_j(t)\frac{RT}{MW_j p_j^0}, \tag{24}$$

$j = 1$ for DBP,

$j = 2$ for DOP.

Measured nucleation rates frequently do not agree with those predicted by classical nucleation theory; thus we introduce a factor to be experimentally determined that brings the two into agreement. That factor E_J can be termed an enhancement factor.[5,17] In general, the enhancement factor is different for different condensing species; a key contribution of this work is the determination of the best-fit enhancement factors for DBP, DOP, and the mixed vapor cases.

IV. COMPARISON OF MEASURED AND PREDICTED NUCLEATION RATES

The experimental data shown in Fig. 5 are repeated in Fig. 7, where the closed symbols again represent the number concentrations of particles observed experimentally. The corresponding open symbols of the same shape are the model predictions for the experimental temperatures and saturation ratios. Also indicated in Fig. 7 are the enhancement factors used in Eq. (22) for the binary, DBP, and DOP nucleation simulations. The value of $E_{\mathrm{DBP}} = 10^7$ used here agrees well with values of the DBP enhancement factor previously observed for conditions of temperature and saturation ratios similar to those used in this study.[5] The model predictions shown in Fig. 7 agree well with the trends in the experimentally observed total number of particles, and can predict closely the total number as well with the appropriate enhancement factor.

A summary of the saturation ratios in all the mixed-vapor cases studied is shown in Fig. 8. Each of these points has a corresponding single-component DBP point and a single-component DOP point that was used for comparison of homomolecular nucleation rates. Many of the measured number concentrations are shown in Figs. 9–11.

The experimental procedure used to obtain the data shown in Fig. 9 was similar to that described previously, but in this case the DOP saturator was maintained at 120 °C as the DBP saturator temperature was varied, resulting in somewhat lower values of saturation ratio than those in Fig. 7. Again, the predicted number concentrations agree within an order of magnitude with those observed, for values of the

Downloaded 21 Dec 2005 to 131.215.225.171. Redistribution subject to AIP license or copyright, see http://jcp.aip.org/jcp/copyright.jsp

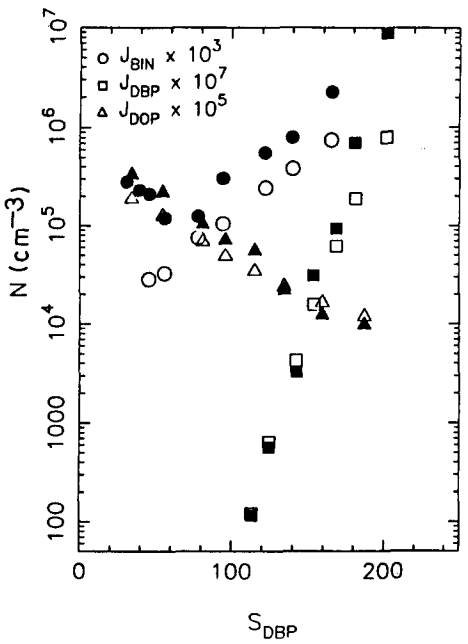

FIG. 7. Predicted and measured total particle number concentrations, T_{sh2} = 130 °C

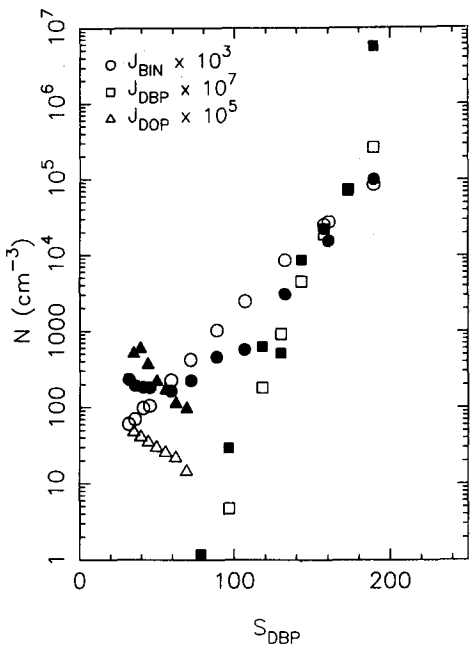

FIG. 9. Predicted and measured total particle number concentrations, T_{sh2} = 120 °C.

enhancement factors $E_{BIN} = 10^3$, $E_{DBP} = 10^7$, and $E_{DOP} = 10^5$.

Figures 10 and 11 show data obtained for constant temperatures in the DBP saturators of 124 and 130 °C, respectively, and stepwise variation of the DOP saturator temperature. The variation of the DOP saturator temperature results in a stronger dependence upon S_{DOP}, and therefore the data are plotted against this abscissa. Similar enhancement factors were used for the binary and DOP simulations, but a slightly smaller enhancement factor ($E_{DBP} = 10^6$) than was found for the experiments shown in Figs. 7 and 9 was required to accurately represent the DBP nucleation data. As in all the studies, the total number concentration of particles measured in the binary vapor system exceeds those expected via homomolecular nucleation alone, except in the case of very small or very large saturation ratio of DOP. For small S_{DOP}, nucleation of DBP alone dominates, and the mixed vapor number concentrations tend towards those found for DBP only. However, in Figs. 10 and 11 it appears that the

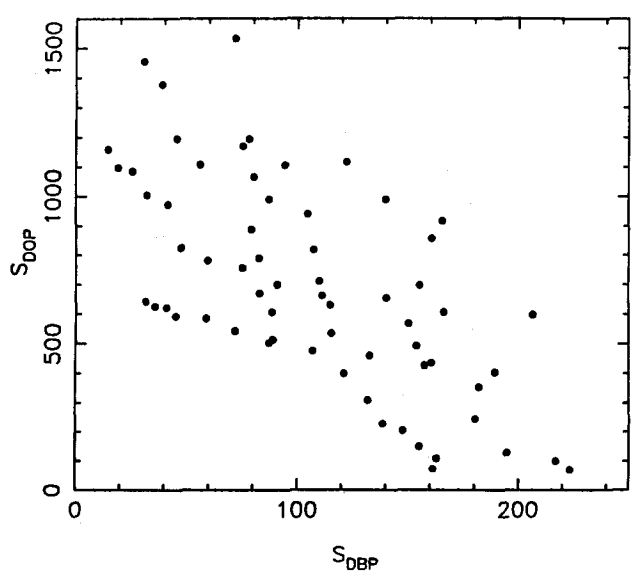

FIG. 8. Summary of binary experiments performed.

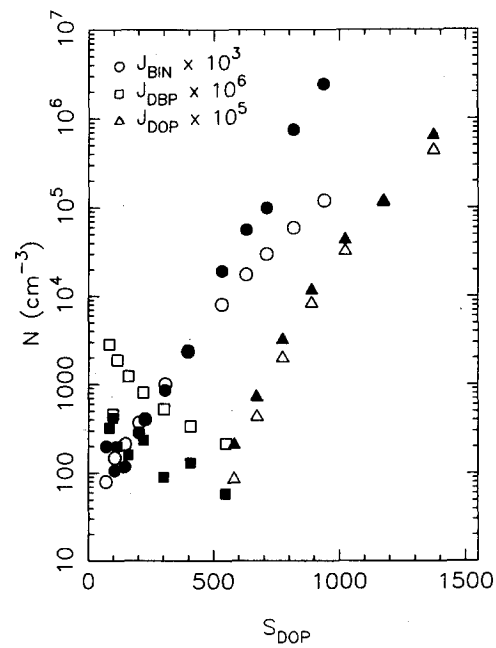

FIG. 10. Predicted and measured total particle number concentrations, T_{sh1} = 124 °C.

Downloaded 21 Dec 2005 to 131.215.225.171. Redistribution subject to AIP license or copyright, see http://jcp.aip.org/jcp/copyright.jsp

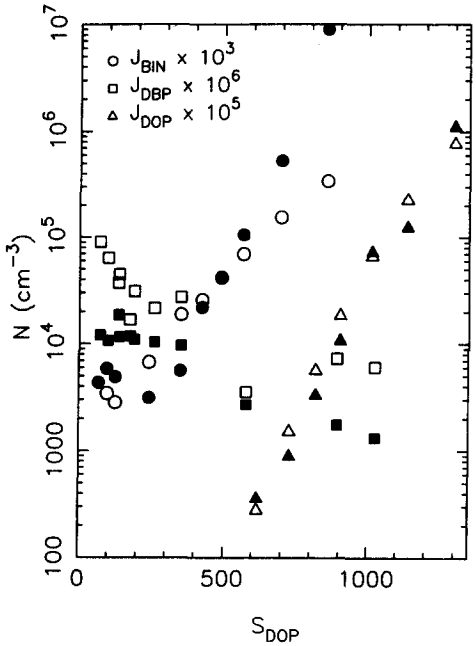

FIG. 11. Predicted and measured total particle number concentrations, $T_{sh1} = 130$ °C.

binary experimental data do not tend towards those for single-component DOP as the saturation ratio of DOP becomes large, although the binary simulations do approach the DOP-only case; the reason for this behavior of the model will be explained in the discussion of the enhancement factor which follows. The reasons for the apparently anomalous behavior of the experimental data may be explained in part by the difficulty of showing a three-dimensional function on a two-dimensional plot. That is, it is not evident from this representation what the saturation ratio of DBP is for the mixed vapor case at high S_{DOP}. If the DBP concentration is still high enough to significantly impact the nucleation rate, the mixed vapor data will not approach the single-component DOP data. In fact, the detection limit of the particle counter is 10^7 cm^{-3}, so that the number concentration at which the binary and single-component DOP curves converge may not be experimentally observable.

The inadequacies of the two-dimensional representation can be clarified by consideration of Figs. 12 and 13, in which the data of Figs. 10 and 11, respectively, have been replotted. In Fig. 12(a), the DBP-only and mixed-vapor results of Fig. 10 are shown as functions of S_{DBP}, and in Fig. 12(b), the DOP-only and mixed-vapor results are shown as functions of S_{DOP}; similar comments apply to Figs. 13(a) and 13(b).

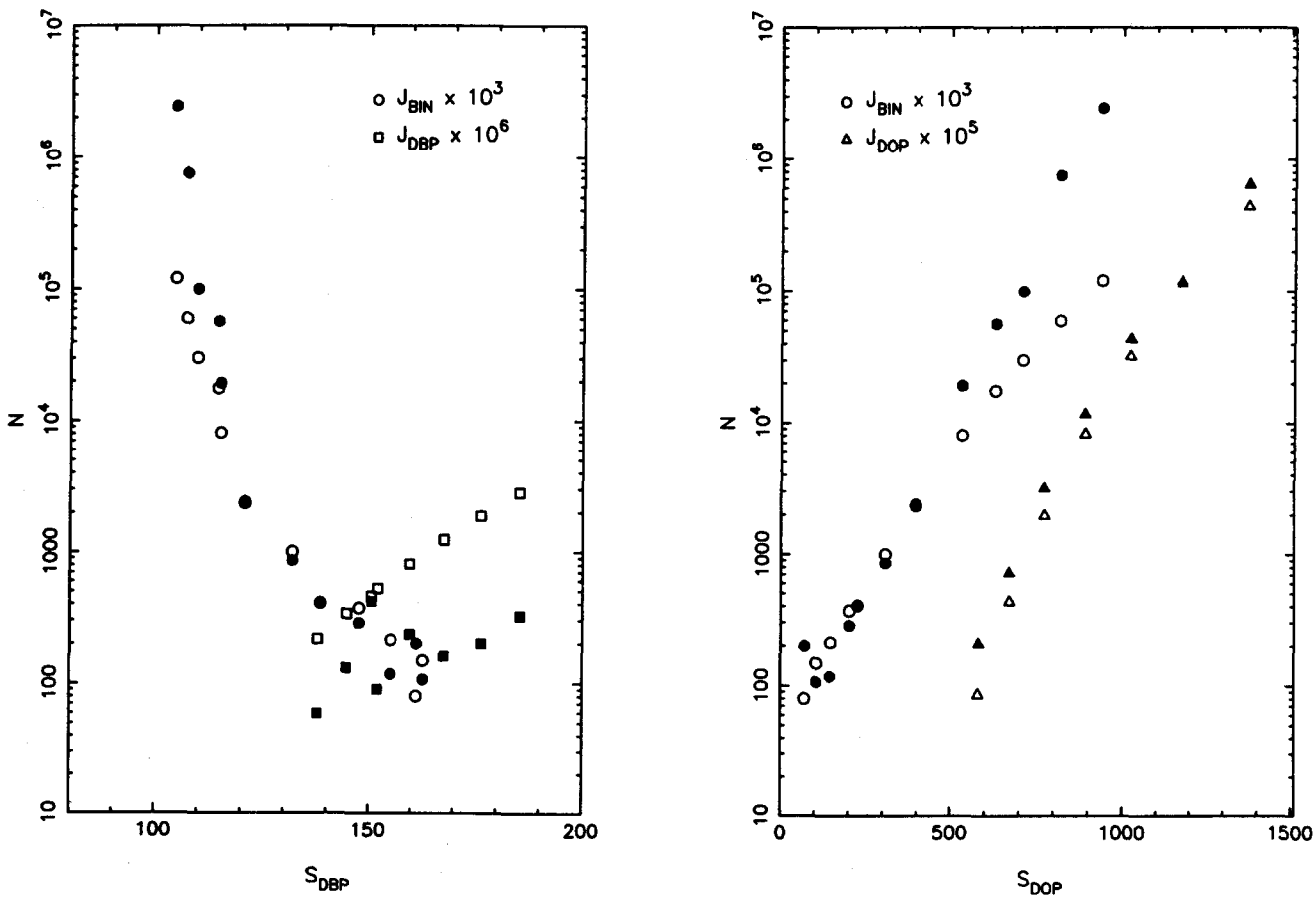

FIG. 12. Predicted and measured total particle number concentrations, $T_{sh1} = 124$ °C.

Downloaded 21 Dec 2005 to 131.215.225.171. Redistribution subject to AIP license or copyright, see http://jcp.aip.org/jcp/copyright.jsp

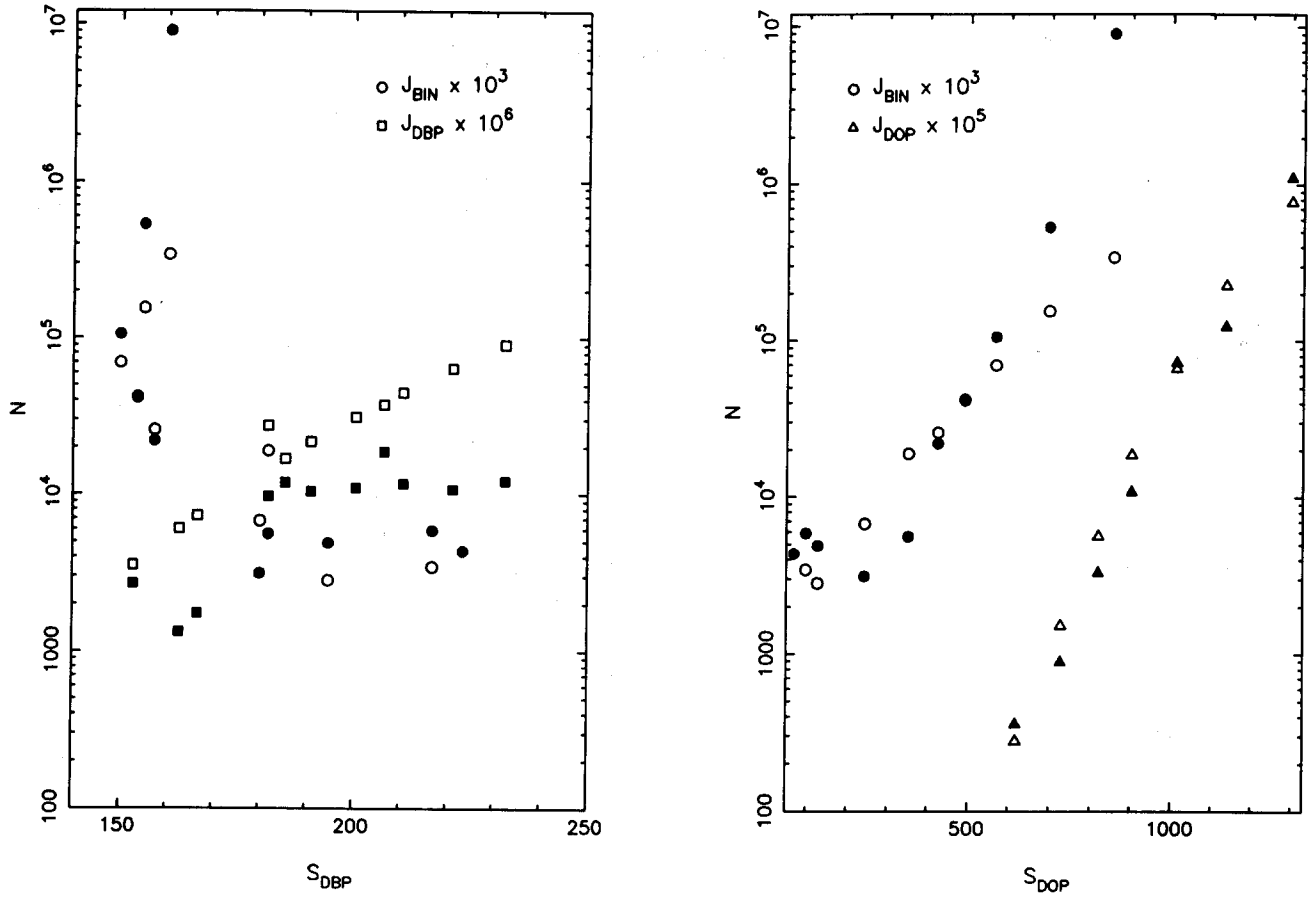

FIG. 13. Predicted and measured total particle number concentrations, $T_{sh} = 130$ °C.

It is now clear, from Fig. 12(a), why the binary data do not tend toward the DOP-only data: the minimum saturation ratio of DBP is about 150, evidently still high enough to affect the binary particle formation. (From Figs. 7 and 9, one sees that DBP is undersaturated with respect to single-component particle formation only below about $S_{DBP} = 100$, so one might expect its effect on the binary rate to be significant even below $S_{DBP} = 100$, depending upon the vapor concentration of DOP; if the concentration of DOP overwhelms that of DBP, single-component nucleation of DOP may dominate kinetically.) These arguments also apply to Figs. 13(a) and 13(b).

The use of an enhancement factor to reconcile theoretically predicted and experimentally observed nucleation rates is at present simply a convenient means for representing such deviations. The enhancement factor found for the mixed-vapor cases, $E_{BIN} = 10^3$, is significantly lower than those found to represent the homomolecular nucleation of either organic. A possible explanation for this observation lies in the assumptions made for the physical properties of the binary solution. The ideal mixture assumption for the molar volume of the solution is probably adequate, and, in any case, the nucleation rate does not depend very strongly on density. The equilibrium calculations will be affected by the values assumed for the activity of each species over the solution; Raoult's Law may not be valid over the full composition range. Probably the most important assumption, however, and the one most likely to be in error, is the surface tension assumed for the liquid mixture. The free energy of the critical cluster, and hence the calculated nucleation rate, is very sensitive to this parameter: a two percent reduction in surface tension can produce an order of magnitude increase in the nucleation rate. The surface tension also affects the magnitude of the Kelvin term, and hence will modify the condensation rate onto existing particles. Since nucleation and condensation are competing processes, errors in σ will also impact the total number of particles that are predicted to be produced.

One of the consequences of using a binary enhancement factor that is much smaller than those used for the single-component species in the model is that the model predictions in the binary case, as the saturation ratio of one component becomes small, will no longer go smoothly to the single-component limit; this can be seen by lowering the $\Delta G = \Delta G^{id}$ curve in Fig. 6 by three orders of magnitude in R_J, and considering its points of intersection with curves *A* and *B*. Similar behavior is found for the model results; in Fig. 7, for example, binary nucleation predictions at low S_{DBP} fall below those of single-component DBP, whereas the binary experiments go smoothly to the single-component experiments in this limit. It is somewhat difficult to obtain the "best-fit" binary enhancement factor, since the mixed-vapor results depend upon two variables. For example, the same binary model and experimental results are shown in Figs. 12(a) and

Downloaded 21 Dec 2005 to 131.215.225.171. Redistribution subject to AIP license or copyright, see http://jcp.aip.org/jcp/copyright.jsp

12(b), but the model appears to fit the data better when shown as a function of S_{DBP} than when plotted against S_{DOP}. A single, nonadjustable factor E_{BIN} may be inadequate to describe the behavior over the entire experimental range.

V. CONCLUSIONS

The particle size magnifier, which has previously been used to study homomolecular nucleation, has been extended to investigate binary nucleation phenomena. This work concerns the binary nucleation of two organic vapors, dibuytlphthalate and dioctylphthalate, for a wide range of saturation ratios. The nucleation behavior of mixed-vapor systems was compared with that observed in the presence of either organic alone. The number of particles formed in the binary case is larger than would be expected via homomolecular nucleation, confirming the interaction between the two organic species during particle formation. In the mixed-vapor case, however, as the saturation ratio of one species became very large or very small, the numbers of particles produced tended towards those observed in the single-vapor cases.

Observed aerosol number concentrations were compared with the predictions of an integral model that allows for competition between nucleation and growth processes in gas-to-particle conversion, and that uses as particle source rates the predictions of classical homomolecular nucleation theory and binary nucleation theory, modified by suitable experimentally determined enhancement factors; a key contribution of this work is the measurement of the DBP, DOP, and binary DBP/DOP enhancement factors. When these enhancement factors are employed, the total number of particles as well as the trends in number concentration with saturation ratio that are predicted compare favorably to those observed experimentally.

ACKNOWLEDGMENT

This work was supported by National Science Foundation Grant No. ATM-8503103.

APPENDIX

1. The parameter α

In this appendix we demonstrate the origin of the condensation equation for a binary aerosol, Eqs. (7) and (8), considering first the appropriate distribution function for a multicomponent aerosol. We show that the correct equation is analogous to that written for homomolecular condensation. We next discuss the origin of the factor α as a correction for the diameter used in the integral model, and show how to calculate α for the special case of a lognormal aerosol for which the Kelvin effect is negligible.

The aerosol size-composition probability density function is defined[18]

$$dN = N_\infty g(m_1,m_2,...,m_k)dm_1dm_2\cdots dm_k, \tag{A1}$$

where N_∞ is the total number of particles and m_i are the moles of species i in a particle. A size distribution function $\tilde{n}(m_1)$ can be obtained by integrating over all but one of the species:

$$\tilde{n}(m_1) = N_\infty \int_{m_2}\cdots\int_{m_k} g(m_1,m_2,...,m_k)dm_2\cdots dm_k. \tag{A2}$$

In the single-component case, the total moles in the aerosol phase are

$$\begin{aligned} M &= \int_{d_p} m(d_p)n(d_p)dd_p \\ &= \frac{\rho\pi}{6}\int_{d_p} d_p^3 n(d_p)dd_p \\ &= \frac{\rho\pi}{6} N_\infty \bar{d}_{p_m}^3, \end{aligned} \tag{A3}$$

where $\bar{d}_{p_m}$ is the mass (or mole) mean diameter. The mass mean diameter is defined as the diameter of a particle having the mean mass of the distribution. This is exactly the definition used to determine $\bar{d}_p$ of Eq. (8).

In the case of a binary aerosol, the total moles of each component must be computed. Considering first species 1,

$$\begin{aligned} M_1 &= \int_{m_1} m_1\tilde{n}(m_1)dm_1 \\ &= N_\infty \int_{m_1}\int_{m_2} m_1 g(m_1,m_2)dm_1dm_2 \\ &= N_\infty \bar{m}_1, \end{aligned} \tag{A4}$$

where M_1 are the total moles of species 1 in the aerosol and $\bar{m}_1$ is the average moles of species 1 per particle.

To determine the change in the total aerosol moles with time for a single-component aerosol,

$$\frac{dM}{dt} = \int_{d_p}\frac{dm}{dt} n(d_p)dd_p, \tag{A5}$$

whereas for the binary case, for species 1,

$$\begin{aligned} \frac{dM_1}{dt} &= N_\infty \int_{m_1}\int_{m_2}\frac{dm_1}{dt} g(m_1,m_2)dm_2dm_1 \\ &= \int_{m_1}\frac{dm_1}{dt}\tilde{n}(m_1)dm_1. \end{aligned} \tag{A6}$$

From the properties of size distributions it can be shown that

$$n(d_p)dd_p = \tilde{n}(m_1)dm_1, \tag{A7}$$

so that Eq. (A6) is equivalent to

$$\frac{dM_1}{dt} = \int_{d_p}\frac{dm_1}{dt} n(d_p)dd_p. \tag{A8}$$

Similar arguments can be used for the change in M_2 with time. Equation (A8) is identical to Eq. (A5) for the single component case, except that in Eq. (A8) the rate of change of mass per particle refers to the condensation rate of species 1 only.

Since the binary and single-component cases are similar, for simplicity we will discuss the factor α referring to the single-component case only. In the discussion that follows the assumption will be made that the Kelvin effect, $\exp(4\sigma V/d_pRT)$, which is the factor by which the vapor pressure over a droplet is enhanced due to the curvature of the surface, is approximately equal to one. For large particles (continuum regime), this assumption is usually a good

Downloaded 21 Dec 2005 to 131.215.225.171. Redistribution subject to AIP license or copyright, see http://jcp.aip.org/jcp/copyright.jsp

one, but it can be in error for small particle sizes or large values of σ. We will consider the two limiting cases of growth in the continuum and kinetic regimes.

2. Continuum regime

The condensation rate onto a single particle is given by

$$\frac{dm}{dt} = \frac{2\pi D p^0}{RT} d_p (S-1). \tag{A9}$$

Note that in the binary case, for component 1, we can write

$$\frac{dm_1}{dt} = \frac{2\pi D_1 p_1^0}{RT} d_p a_1 \left(\frac{S_1}{a_1} - 1\right). \tag{A10}$$

Summing over all diameters of the distribution, the total rate of change of moles is

$$\frac{dM}{dt} = \frac{2\pi D p^0}{RT} (S-1) \int_{d_p} d_p n(d_p) dd_p$$

$$= \frac{2\pi D p^0}{RT} (S-1) N \bar{d}_{p_n}, \tag{A11}$$

where $\bar{d}_{p_n}$ is the number mean diameter of the distribution. Using the definition of α given in Eqs. (7) and (8),

$$\frac{dM}{dt} = \frac{2\pi D p^0}{RT} (S-1) \alpha N \bar{d}_{p_m}. \tag{A12}$$

Comparison of Eqs. (A11) and (A12) shows that α is given by

$$\alpha_c = \bar{d}_{p_n} / \bar{d}_{p_m}. \tag{A13}$$

3. Kinetic regime

The condensation rate onto a single particle is given by

$$\frac{dm}{dt} = \frac{\bar{c}\pi p^0}{RT} d_p^2 (S-1), \tag{A14}$$

with the total rate onto all particles

$$\frac{dM}{dt} = \frac{\bar{c}\pi p^0}{RT} (S-1) \int_{d_p} d_p^2 n(d_p) dd_p$$

$$= \frac{\bar{c}\pi p^0}{RT} (S-1) N \bar{d}_{p_s}, \tag{A15}$$

where $\bar{d}_{p_s}$ is the surface area mean diameter of the distribution. By comparison with the expression used in the integral model, it can be shown that in this case

$$\alpha_k = (\bar{d}_{p_s} / \bar{d}_{p_m})^2. \tag{A16}$$

4. Magnitude of α

Equations (A13) and (A16) can be written

$$\alpha_c = \frac{\int_0^\infty d_p n(d_p) dd_p}{\left[\int_0^\infty d_p^3 n(d_p) dd_p\right]^{1/3}}, \tag{A17}$$

$$\alpha_k^{1/2} = \frac{\left[\int_0^\infty d_p^2 n(d_p) dd_p\right]^{1/2}}{\left[\int_0^\infty d_p^3 n(d_p) dd_p\right]^{1/3}}. \tag{A18}$$

For simplicity in the following analysis, let $x = d_p$ and consider a normalized distribution function $n(x)$, so that

$$\int_0^\infty n(x) dx = 1. \tag{A19}$$

We will make use of Hölder's inequality, where $1/p + 1/q = 1$:

$$\int_a^b |f(x)g(x)| dx \leqslant \left(\int_a^b |f(x)|^p dx\right)^{1/p} \left(\int_a^b |g(x)|^q dx\right)^{1/q}. \tag{A20}$$

In applying Eq. (A20), the absolute value signs will be omitted, since the distribution functions we consider are always positive.

Using Hölder's inequality with $f(x) = x n(x)^{1/3}$, $g(x) = n(x)^{2/3}$, $p = 3$, and $q = 3/2$,

$$\int_0^\infty x n(x) dx \leqslant \left(\int_0^\infty x^3 n(x) dx\right)^{1/3} \left(\int_0^\infty n(x) dx\right)^{2/3}. \tag{A21}$$

The last term in Eq. (A21) is equal to unity [Eq. (A19)]. Thus we obtain the relation

$$\alpha_c = \frac{\int_0^\infty x n(x) dx}{\left[\int_0^\infty x^3 n(x) dx\right]^{1/3}} \leqslant 1. \tag{A22}$$

Similarly, applying Eq. (A20) with $f(x) = x^2 n(x)^{2/3}$, $g(x) = n(x)^{1/3}$, $p = 3/2$, and $q = 3$,

$$\int_0^\infty x^2 n(x) dx \leqslant \left(\int_0^\infty x^3 n(x) dx\right)^{2/3} \left(\int_0^\infty n(x) dx\right)^{1/3}, \tag{A23}$$

from which one obtains

$$\alpha_k^{1/2} = \frac{\left[\int_0^\infty x^2 n(x) dx\right]^{1/2}}{\left[\int_0^\infty x^3 n(x) dx\right]^{1/3}} \leqslant 1. \tag{A24}$$

The factor α is less than one, or equal to one in the case of a monodisperse aerosol, for any continuous distribution function, and the assumption of monodispersity therefore maximizes the condensation rate.

In the special case of a lognormal aerosol, α can be written in terms of the variance of the distribution, σ_g:

$$\alpha_c = \alpha_k = \exp(-\ln^2 \sigma_g). \tag{A25}$$

It is seen that $\alpha = 1$ is true only in the case of a monodisperse aerosol, for which the variance is equal to unity. For a lognormal aerosol with $\sigma_g = 1.3$, $\alpha = 0.93$. Thus the assumption of monodispersity results in a condensation rate about 7% too large.

[1] H. Reiss, J. Chem. Phys. **18**, 840 (1950).
[2] H. Reiss, D. I. Margolese, and F. J. Schelling, J. Colloid Interface Sci. **56**, 511 (1976).
[3] P. Mirabel and J. L. Clavelin, J. Chem. Phys. **68**, 5020 (1978).
[4] W. Studzinski, G. H. Spiegel, and R. A. Zahoransky, J. Chem. Phys. **84**, 4008 (1986).
[5] K. Okuyama, Y. Kousaka, D. R. Warren, R. C. Flagan, and J. H. Seinfeld, Aerosol Sci. Technol. **6**, 15 (1987).
[6] D. R. Warren, K. Okuyama, Y. Kousaka, J. H. Seinfeld, and R. C. Flagan, J. Colloid Interface Sci. **116**, 563 (1987).
[7] D. R. Warren and J. H. Seinfeld, Aerosol Sci. Technol. **3**, 135 (1984).
[8] D. R. Warren and J. H. Seinfeld, J. Colloid Interface Sci. **105**, 136 (1985).

Downloaded 21 Dec 2005 to 131.215.225.171. Redistribution subject to AIP license or copyright, see http://jcp.aip.org/jcp/copyright.jsp

[9]S. M. Kreidenweis and J. H. Seinfeld, Atmos. Environ. **22**, 283 (1988).
[10]B. Dahneke, in *Theory of Dispersed Multiphase Flow* (Academic, New York, 1983).
[11]P. Mirabel and J. L. Katz, J. Chem. Phys. **60**, 1138 (1974).
[12]D. Stauffer, J. Aerosol Sci. **7**, 319 (1976).
[13]P. Ravindran and E. J. Davis, J. Colloid Interface. Sci. **85**, 278 (1982).
[14]G. Wilemski, J. Chem. Phys. **80**, 1370 (1984).
[15]G. Wilemski, J. Chem. Phys. **62**, 3763 (1975).
[16]P. Mirabel and J. L. Clavelin, J. Aerosol Sci. **9**, 219 (1978).
[17]R. Strey, P. E. Wagner, and T. Schmeling, J. Chem. Phys. **84**, 2325 (1986).
[18]S. K. Friedlander, *Smoke, Dust and Haze* (Wiley, New York, 1977).

Downloaded 21 Dec 2005 to 131.215.225.171. Redistribution subject to AIP license or copyright, see http://jcp.aip.org/jcp/copyright.jsp